RESEARCH PAPER

Measuring flow velocity distribution in microchannels using molecular tracers

Cuifang Kuang · Wei Zhao · Fang Yang · Guiren Wang

Abstract We demonstrate the capability of a molecular tracer based laser induced fluorescence photobleaching anemometer for measuring fluid velocity profile in microfluidics. To validate the feasibility and accuracy of this measurement system, the velocity profiles of the cylindrical and rectangular microchannels are measured, respectively. We compare our experimental results with theoretical prediction. The theoretical prediction shows a good consistency with practical measurement results. The spatial resolutions are analyzed and validated. Finally, the error source of the presented system is analyzed, which makes it possible to compensate some error quantitatively and guides the application of this system.

1 Introduction

Microfluidic devices have drawn a great attention over the last decade due to the development of an increasing number of applications in biomedical diagnosis and chemical analysis. Microfluidic technology has the potential to significantly change the way modern biology, chemistry, biomedicine and biotechnology are performing. Although the flow mostly remains laminar in microchannels system,

C. Kuang · W. Zhao · F. Yang · G. Wang (✉)
Department of Mechanical Engineering and Biomedical
Engineering Program, University of South Carolina,
Columbia, SC 29208, USA
e-mail: guirenwang@sc.edu

physical measurement should still play an important role in the analysis of the flow field. For instance, since bio-fluid flows often exhibit no-Newtonian characteristics, the numerical analysis sometimes becomes difficult (Angele et al. 2005).

There are many techniques to measure the velocity profile in microchannels for either pressure driven flow or electroosmotic flow (EOF). Sampling weighing (Guenat et al. 2001; Altria and Simpson 1987) can measure the bulk velocity, but could be less accurate due to evaporation and sensitivity of the balance. In conductivity cell (Liu et al. 2001; Wanders et al. 1993) and current monitoring (Huang et al. 1988; Chien and Helmer 1991) average EOF is measured by observing changes in current and conductivity versus time, respectively. The methods mentioned cannot measure velocity profile of the tubing. Another method is based on the NMR (Tallarek et al. 2000), which can measure the velocity profile. Unfortunately, this method has relatively low spatial resolution (Wu et al. 1995; Manz and Stilbs 1995; Gladden 2003).

Many velocimeters use optical techniques, mainly because they are non-invasive for measuring the flow field. These optical measurement methods can be classified into three categories: measuring flush time, particle tracers and molecular tracers. The easiest method to measure the flow velocity is the tracking neutral markers by measuring the flush time of a neutral marker from injection to detection point (Sandoval and Chen 1996; Williams and Vigh 1997). However, this method cannot measure velocity profile. For the particle tracer methods, several techniques are used to acquire velocity profile. Such as laser Doppler velocimetry (LDV) (Aksel and Schmidtchen 1996), particle streak velocity (PSV) (Dahms et al. 2007), particle tracking velocimetry (PTV) (Sato et al. 2003) and particle image velocimetry (PIV) (Sinton 2004). The most widely used

method is PIV. This method has been successfully extended to microscale flows by combining the conventional PIV with microscopy, therefore, it is known as μPIV (Koutsiaris et al. 1999; Meinhart et al. 1999; Klank et al. 2002; Sugii et al. 2002; Chiu et al. 2003; Devasenathipathy et al. 2003; Shinohara et al. 2004) with confocal microscopy, known as confocal scanning μPIV (Park et al. 2004; Lima et al. 2006; Kinoshita et al. 2005), and so was the PIV at near wall (Zettner and Yoda 2003; Jin et al. 2004). Even though the PIV is a very successful method, the measurement system is relatively complex and expensive, and in some case, the seed particles are undesirable, since they may interfere with the flow field. This is particularly true when the fluidic channel is in submicron meter range. There are also situations in which the inertia and buoyancy of the particles can compromise their ability to track the fluid motion.

Molecular tracers' approaches can offer significant advantages. The measured displacement of tagged regions provides the estimate of the fluid velocity vector. One might think of the MTV technique as the molecular counterpart of PIV. Koochesfahani and Nocera (2001) and Hu and Koochesfahani (2006a, b) presented a method based on water-soluble phosphorescent supramolecules and a planar grid of intersecting laser beams. Ross et al. developed another molecular tracer method based on caged-fluorescence visualization (Ross et al. 2001). While the said two molecular tracers based methods can measure velocity profile in microchannels, their temporal resolution could be relatively low, since they measure 2D flow field directly. On the other hand, several molecular tracer methods based on photobleaching were presented. Mosier et al. (2002) and Flamion et al. (1991) proposed the photobleached-fluorescence imaging and fluorescence photobleaching recovery methods, respectively. However, the former has difficulty in measuring velocity profile directly and the later has relatively low temporal resolution (about 80 ms measurement time at the 40 nl/min flow rate) as it has to wait for the recovery of fluorescence intensity. Method using two detecting windows based on photobleaching was developed by Schrum et al. (2000) and Pittman et al. (2003). Although this method is subtle and relatively simple, it has lower temporal resolution and cannot measure velocity profile. Recently, Wang et al. (Wang 2005; Wang et al. 2008) proposed another molecular tracer method for measuring the velocity in microchannel based on laser induced fluorescence photobleaching anemometer (LIFPA), but the presented system cannot measure the velocity profile of the microchannels. The goal of the present work is to develop a single point measuring method based on LIFPA and epi-fluorescence structure, which could easily measure flow velocity profile with high spatial resolution and potentially high temporal resolution (Kuang

et al. 2008). To accomplish this, we investigate its ability to study the velocity distribution in both cylindrical and rectangular microchannels.

2 Measurement principle and system configuration

2.1 System configuration

The following section will describe the principle of measurement used in the system and the system configuration as well. Figure 1 shows a schematic diagram of the experimental setup. This system is similar to an epi-fluorescence structure. The optical setup of the measurement system consists of an excitation wavelength of 405 nm laser beam from a violet laser (Crystalaser Corp.), a beam expander (5×), a dichroic mirror Z405RDC (Chroma Corp.), an oil-immersion objective having a magnification of 100 and numerical aperture NA = 1.3 (Olympus Corp.), a 10 μm pinhole, a photodiode detector, and a narrow band filter HQ460/50 M (Chroma Corp.), respectively. The microchannel was placed on a 3D piezoelectric nanopositioning stage E-664 (Physics Instrument). A Harvard syringe pump (PHD 2000) is used to drive the fluid with a syringe containing fluorescence dye solution.

2.2 Materials

The present measurement method is based on photobleaching and the stronger the photobleaching, the higher the sensitivity (Wang 2005; Wang et al. 2008). A neutrally charged dye coumarine 102 (Sigma-Aldrich Corp.) is used, which has a relatively high quantum efficiency of photobeaching and has a high absorption coefficient at about 400 nm wavelength and emission around 460 nm wavelength (Eggeling et al. 1998). The dye was diluted with pure methanol solution to a concentration of 100 μM with a HEPES 20 mM buffer solution.
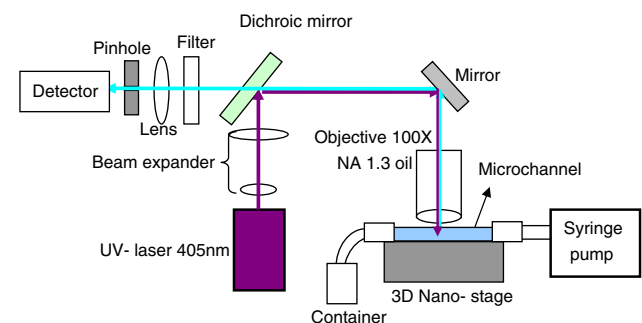
Fig. 1 Schematic diagram of the measuring system based on epi-fluorescence structure

2.3 Measurement mechanism

The measurement principle is based on LIFPA (Wang 2005; Wang et al. 2008). While the earlier work can measure the bulk velocity, it cannot measure the velocity profile of the microchannels. However, in many case, the velocity profile plays a key role for transport phenomena in microchannels. In order to measure velocity profile in microchannels, the high spatial resolution measurement system is required. For this purpose, we developed a LIFPA system that is able to measure velocity profile based on epi-fluorescence and confocal microscopy. Current LIFPA method developed is a single point measurement. If the flow velocity is slow, the dye in the flow will have a longer residence time in the laser beam at the detection point, causing a longer photobleaching time. The residence time within the detection region is approximately equal to the photobleaching time. The longer the photobleaching time, the smaller the fluorescence signal. Thus, the fluorescence intensity increases with the flow velocity. We can first calibrate the relationship between the fluorescence signal and a known velocity. The higher the velocity, the higher the fluorescence signal. For very low flow velocity, the fluorescence signal can be linearly related to the flow velocity. With the calibration curve, the velocity can easily be calculated by measuring fluorescence intensity only.

It is well known that photobleaching can be simplified as an exponent decay of fluorescence intensity I_f with time t (Pernoder and Tinland 1997; Flamion et al. 1991; Champion et al. 1995

$$I_f = I_0 e^{-t/\tau} \tag{1}$$

where I_0 represents fluorescence intensity at $t = 0$; τ denotes the photobleaching time constant, e.g. half decay time, which can be determined through experiment. Suppose the focus spot through an objective is approximately like a small cube shown in Fig. 2, fluid velocity is V, S is area perpendicular to the fluid velocity the focus spot width is L. After time t, if the residence position of the entrance dye is x in this cube, then

$$t = x/V \tag{2}$$

$$I_f = I_0 e^{-x/(V\tau)} \tag{3}$$

Suppose the fluorescence excited is received by a detector in this cube. The fluorescence intensity received can be expressed as

$$I = KS \int_0^L I_f dx \tag{4}$$

where K is the photoelectric conversion factor. Combining Eqs. (3) and (4) we obtain
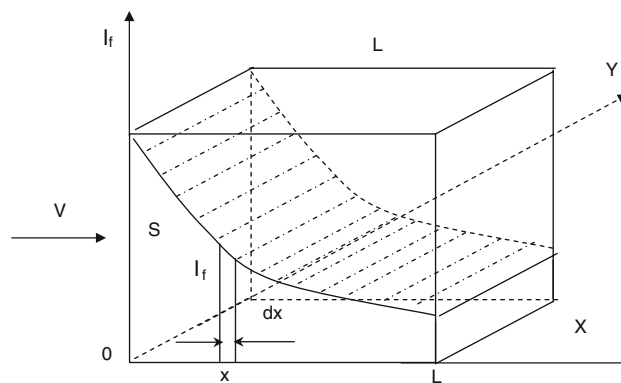

Fig. 2 Schematic diagram of a dye solution passing through a focus spot of laser
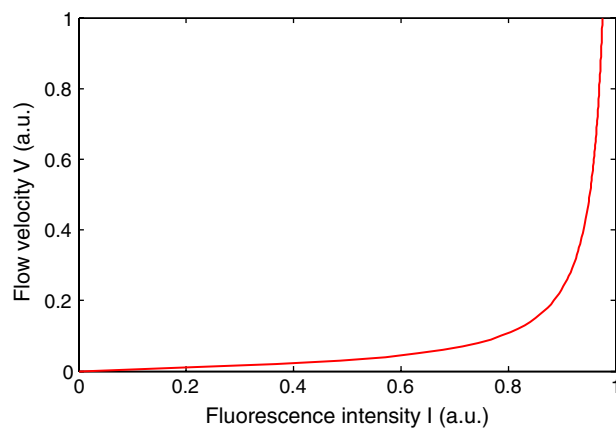

Fig. 3 The relationship (normalized) between flow velocity and fluorescence intensity by theoretical simulation. Here, the magnification factor K is 1×10^{16}, the parameter S is 1×10^{-12} m^2, the focus spot width L is 1×10^{-6} m and the half decay time τ is 2 ms. Computed with Eq. 5

$$I = KSI_0 V\tau(1 - e^{-L/(V\tau)}) \tag{5}$$

To illustrate the behavior suggested by (Eq. 4) we show in Fig. 3 the numerical simulation relationship between fluorescence intensity and flow velocity through that cube. The relationship is non-linear in Fig. 3. Therefore, we can initially calibrate the relationship between flow velocity and fluorescence intensity through the measurement of fluorescence intensity I for a known velocity. LIFPA provides us with an easy, fast, instantaneous, accurate and potentially in-line velocity (or flow rate) measurement.

3 Experimental results and analysis

It is a general practice to use a well-known Newtonian fluid to evaluate the performance of a new measurement technique. Two difference shape microchannels (cylindrical and rectangle) were used for the experiments.

3.1 Velocity profile in a cylindrical microchannel

3.1.1 Theoretical foundation

We consider the case of a Newtonian fluid by solving the Navier–Stokes equation with a constant pressure gradient along the axial direction of the microchannel and considering no slip boundary condition at the wall. We obtain the following velocity field equation as a function of position within the cross section of the microchannel and applied gradient (Fournier 2007).

$$V(r) = \frac{\Delta P R^2}{4\mu L}\left[1 - \left(\frac{r}{R}\right)^2\right] \quad (6)$$

$$Q = \frac{\pi R^4 \Delta P}{8\mu L} = \overline{V}\pi R^2 \quad (7)$$

where V is the fluid velocity in axis direction, μ denotes the fluid kinematic viscosity, L the length of the microchannel, ΔP the pressure drop, R the radius of the tube, Q the volumetric flow rate and $\overline{V}$ is the bulk average velocity in the tube. The Eq. (6) describes the velocity profile for laminar tube flow of Newtonian fluids and predicts that the velocity profile has a parabolic shape. By combining Eqs. (6) and (7), it is possible to obtain a very useful expression for maximum velocity in the center of the cylindrical tube. The center velocity of the tubing can be expressed as

$$V_{\text{center}} = 2\overline{V} \quad (8)$$

Thus, we can calibrate the relationship between the velocity and fluorescence intensity using Eqs. (5) and (8). There are some prerequisites for this calibration: (1) the measured flow must be a steady flow; (2) the shape of tube measured must be symmetrical; (3) the parameters of the measurement system (e.g. laser power, dye concentration, and objective, etc.) should not be changed. A calibration curve is universal only when the parameters of the measurement system are fixed. The velocity profile of theoretical prediction (Eq. 6) can be further expressed as

$$V(r) = \frac{2Q}{\pi R^2}\left[1 - \left(\frac{r}{R}\right)^2\right] \quad (9)$$

3.1.2 Experimental analysis

To validate the feasibility and accuracy of this measurement system, a series of experiments were performed under the laboratory conditions. All of the parts of the presented system were fixed on an optical table. Table 1 shows the experimental parameters for the present system. The tested capillary tubing is 75 µm ID and 150 µm OD, which is made with fused silica glass from Polymicro Technologies Corp.

Table 1 Experimental parameters used in this section

|	
Diameter of the cylindrical microchannel	75 µm
Flow rate	1.6 µL/min
Magnification (M)	100×
Numerical aperture	1.3 Oil
Beam expander	5×
Pinhole diameter	10 µm
Excitation wavelength	405 nm
Emission wavelength	∼460 nm
Dye concentration	100 µM
Laser power	20 mW
Optical filter	460 ±25 nm
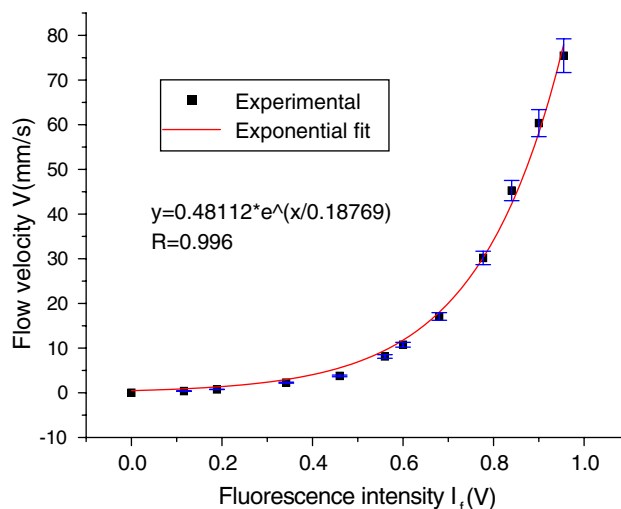
Fig. 4 Calibrated relationship between fluorescence intensity and flow velocity measured in the centerline of the microchannel

Figure 4 shows the experimentally measured relationship between flow velocity V and observed fluorescence intensity I_f. Rectangular dots represent the measured result for the calibration between V and I_f. The line is a calibration curve of the exponential fitting based on the measured V and I_f. Three runs were replicated for each measuring point to generate the averaged curve in Fig. 4. Based on the experimental data in Fig. 4, an exponential fitting or using polynomial fitting (Wang 2005) of the calibration relation for the current setup was obtained

$$V = 0.48112 e^{(I_f/0.18769)} \quad (10)$$

The error bar is the SD. The average relative SD is about 5%. Figure 4 shows that the sensitivity decreases with the increase of V.

Figure 5 is a schematic diagram of scanning directions (horizontal and vertical direction). Two scanning directions were studied, respectively. Figure 6 compares the
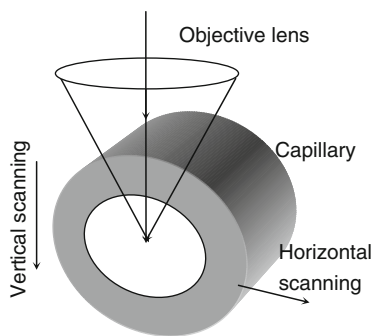
Fig. 5 Schematic of two scanning directions

theoretical prediction using Eq. (10) with the parabolic fitting of the measured data. When the measuring points are scanned horizontally at a rate of 16 μm/s and the sampling rate of 1 kHz with the A/D converter, there is general agreement in the velocity distribution between the experimental result and theoretical prediction as shown in Fig. 6a. The residuals near the two sides of the tubing wall are much larger than that around the centerline of the tube. The maximal error is 1.33 mm/s in the range of 0–12 mm/s. The main error source is the refraction index mismatch, which may result in total reflection near the wall. The reason will be analyzed in detail in Sect. 3.4. On the other hand, when the measuring points are scanned vertically, the agreement between the experimental and theoretical results is much better than that when the measuring points are scanned horizontally as shown in Fig. 6b. The difference is around 2% between the parabolic fitting and theoretical prediction near to the axial region of the tubing. For the entire cross-section measurement, the maximal error is about 0.24 mm/s in the range of 0–12 mm/s, and the average relative SD is less than 3%.
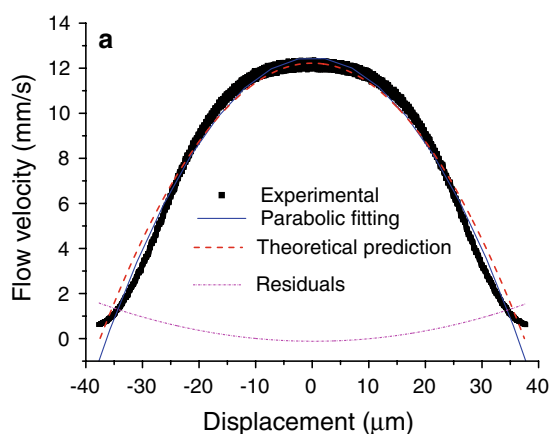
3.2 Velocity profile of a rectangular microchannel

3.2.1 Theoretical foundation

Rectangular microchannels have become very popular for studying flow phenomena in vitro under physiological flow conditions (Lima et al. 2006). In the rectangular microchannel, there is a 1D steady laminar Poiseuille flow in axial direction. By solving the Navier–Stokes equation with a constant pressure gradient along the rectangular microchannel and considering no slip boundary conditions at the wall, it is possible to obtain a useful expression for calculating the velocity profile for the Poiseuille flow in the rectangular microchannel. The velocity field can be expressed as (Lima et al. 2006)

$$V = \frac{48Q}{\pi^3 hw} \frac{\sum_{n,\text{odd}}^{\infty} \frac{1}{n^3} \left[1 - \frac{\cos h(n\pi y/h)}{\cos h(n\pi w/(2h))} \right] \sin(n\pi z/h)}{\left[1 - \sum_{n,\text{odd}}^{\infty} \frac{192h}{n^5 \pi^5 w} \tan h(n\pi w/(2h)) \right]} \quad (11)$$

where w and h are the width and height of the rectangular microchannel, respectively; Q is the corresponding flow rate.

3.3 Experimental analysis

A PDMS channel of 80 μm in width and 45 μm in depth was used in the experiment. The syringe pump provides a nominally constant flow rate of dye solution under 1.2 μl/min and the measurements were carried out at centerline of the channel under steady flow conditions for calibration. Due to the PDMS channel has 1 mm thickness crown glass substrate, the optical setup (Fig. 1) was changed with an objective having a magnification of 40× and NA = 0.6. It has a relatively large working distance (about 4 mm). We measured the velocity profile in this rectangular
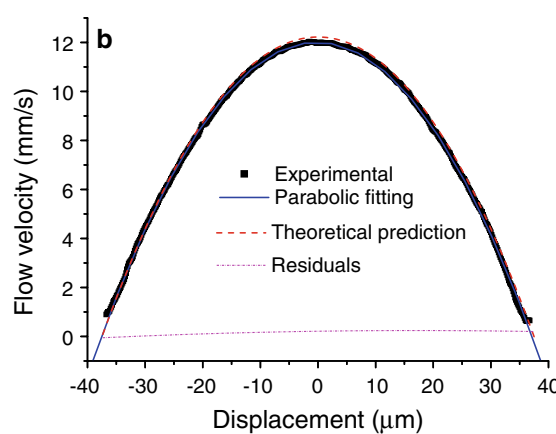
Fig. 6 Comparison of the measured velocity profile (*dots*) of cylindrical microchannel with the parabolic fitting (*solid*) and theoretical prediction (*dash*). Residual errors (*dash dot*) between the theoretical prediction and parabolic fitting data are plotted. **a** Measuring points are scanned horizontally; **b** measuring points are scanned vertically
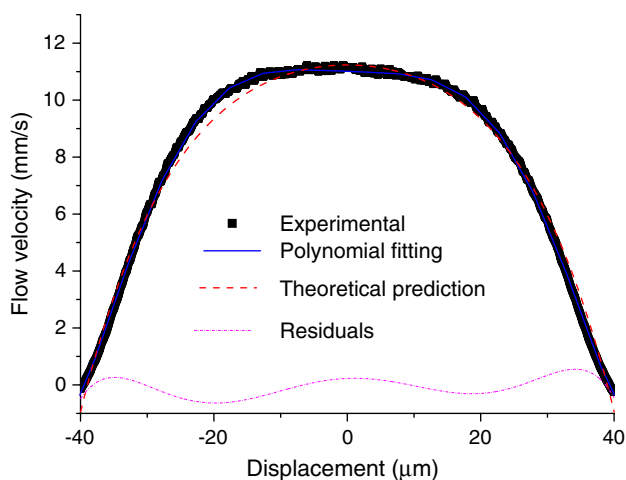
Fig. 7 Comparison of the measured velocity profile (*dots*) of rectangular microchannel with the parabolic fitting (*solid*) and theoretical prediction (*dash*). Residual errors (*dash dot*) between the theoretical prediction and parabolic fitting data are plotted as well

microchannel after the measuring system was calibrated. Figure 7 shows the flow velocity profile of the rectangular microchannel. The velocity profile agrees well with the theoretical prediction for the present system, with deviation on the left-hand side. The majority of the deviations may come from the geometrical uncertainty. Another error source could come from that the cross section of the channel measured might have an inclination away from the horizontal direction. For the entire cross-section measurement, the maximum absolute error is 0.63 mm/s in range of 0–11 mm/s and the average relative SD error is less than 4%.

3.4 Measurement resolution analysis

The presented LIFPA has potential to achieve measurement of ultra high temporal resolution (Kuang et al. 2008) and high spatial resolution simultaneously, since it is based on a single point measurement and requires neither the recovery of fluorescence intensity nor the displacement of fluid or particle. The high spatial resolution can be demonstrated through said two experiments. The setup used in the present experiment is similar to a confocal microscope system, and the spatial resolution is determined by the size of the focused laser beam. If the pinhole size is larger than the Airy unit, we can calculate the spatial resolution by the analysis of geometrical optics (Park et al. 2004). The spatial resolution of the system can be determined by the following equations (Lima et al. 2006):

$$R_1 = \frac{0.51\lambda_{ex}}{NA}; \quad R_a = \frac{0.88\lambda_{ex}}{n - \sqrt{n^2 - NA^2}} \quad (12)$$

where R_1, R_a and n are the lateral resolution, the axial resolution and the refractive index of the solution,

respectively. Thus, according to (Eq. 12), we can get spatial resolution better than 0.2 and 0.4 μm in the lateral and axial direction, respectively, in the experimental system (NA = 1.3). The temporal resolution of the presented system is about 100 μs (Kuang et al. 2008).

3.5 Error analysis

In this section, we will analyze the error sources of proposed measurement system. For horizontal scanning direction, first, the geometric shape of tubing and the refraction index mismatch are the dominating error sources during the measurement. Figure 8 shows the cross section of the cylindrical microchannel. Suppose the angle of incidence of the ray centerline is α_1, the angle of refraction is β_1 in the first interface; the angle of incidence and refraction in the second interface are α_2 and β_2, respectively; n_1, n_2 and n_3 are the refractive index of immersion oil, fused silica and dye solution, respectively; R_1 and R_2 is the outside diameter and inside diameter of the tube, respectively. In according to the Snell's law (Tureci and Stone 2002) and geometric-optical analysis, it was possible to calculate the actual position of focus spot of the system by applying the following equation:

$$x_2 \approx \frac{n_1 x_1}{n_3 \cos(\beta_1 - \alpha_1) \cos(\beta_2 - \alpha_2)} \quad (13)$$

where x_1 and x_2 is nominal and actual position (focus) in the scanning direction. R_1 and R_2 are hidden variables of the trigonometric function in Eq. (13). The refractive index mismatching among the fluid (methanol, $n_3 = 1.329$), the microtube wall (fused silica, $n_2 = 1.458$), and the
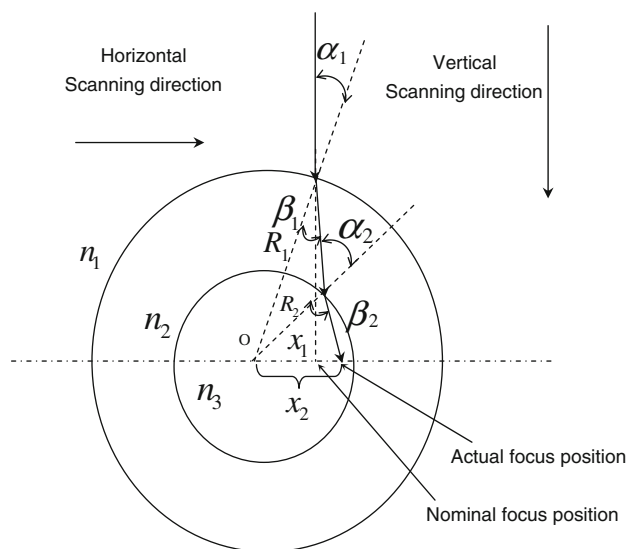
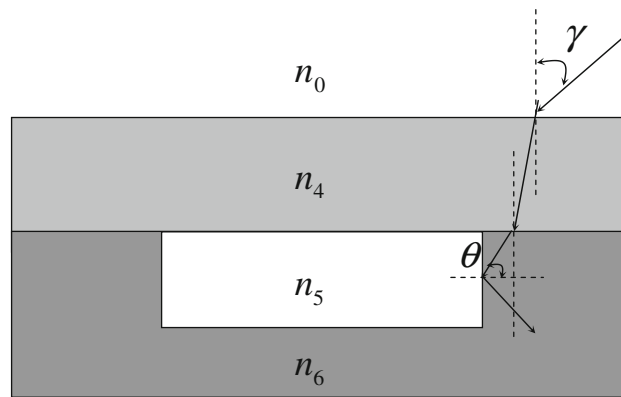**Fig. 8** The schematic illustration of the central ray trajectory
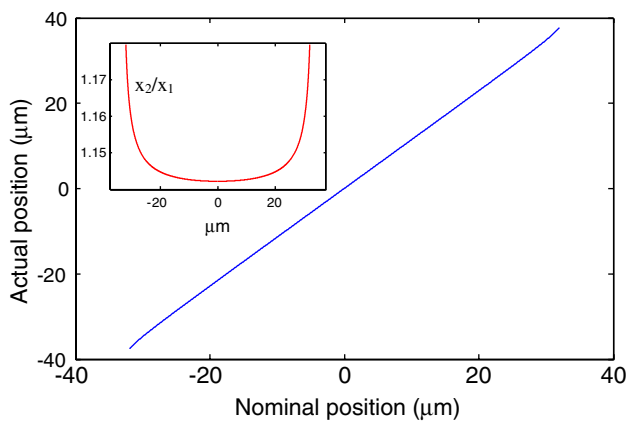
Fig. 9 Test of the approximation underlying (Eq. 13). The *inset* curve is the ratio of the actual position to the nominal position. The following parameters were used: $R_1 = 75$ μm, $R_2 = 37.5$ μm

immersion liquid (oil, $n_1 = 1.518$) contacted to the objective, makes it necessary to compensate for correcting the focus spot position in the scanning direction. The analysis allows correction for actual positioning. Equation (13) is an approximate analysis. We show in Fig. 9 the comparison between the nominal and actual position in horizontal scanning direction. From the inset curve in Fig. 9, we can see the ratio of the actual position to the nominal position is increasing gradually near the wall of the microtube. In doing so, we just have ignored the effect of vertical direction on the actual position of the focus spot. Actually, the along the vertical direction the deviation progressively increases with the radial distance for the center point (Park et al. 2004). However, there is almost not said error source in vertical scanning direction.

On the other hand, the total internal reflection phenomenon is partially generated on the interface near the wall due to the refraction index of n_2 is larger than n_3 and the angle of incidence would be larger than the optical critical angle, which affects the intensity of the excitation light, that is, it affects the velocity measurement. From said analysis which can interpret the relative large deviation near the microtube wall, the error caused by total reflection and non-linear translation of focus spot (inset of Fig. 9) can be significantly suppressed if suitable immersion oil, dye solution and microtube materials were chosen, so that their refractive index match with from each other.

For the rectangular microchannel, there is also total reflection phenomenon near the wall, but no error caused by geometric shape of tubing and refraction index mismatch. The schematic illustration is shown in Fig. 10. According to Snell's law, the critical angle θ at the interface between the dye solution and PDMS shown in Fig. 10 can be expressed as:

Fig. 10 The schematic illustration of the cross section of rectangular microchannel

$$\theta = \sin^{-1}(n_5/n_6) \tag{14}$$

and the incidence angle γ can be expressed as:

$$\gamma = \arcsin\left[\frac{n_6}{n_0}\sqrt{1 - \left(\frac{n_5}{n_6}\right)^2}\right] \tag{15}$$

where $n_0 = 1$, $n_4 = 1.55$, $n_5 = 1.329$ and $n_6 = 1.43$ are refraction index of air, crown glass, dye solution and PDMS material, respectively. So, the incidence angle γ is about 31.9° given by (Eq. 15). Since the NA of the objective is 0.6, the semi-aperture angle is estimated to be 36.9°, which is slightly larger than incidence angle γ. This indicates that the total reflection can occur near the two side walls of the channel.

4 Conclusions

The experimental study shows that the optical techniques, i.e. LIFPA, can be used to measure fluid velocity distribution in the transverse direction of the microchannels with high spatial and temporal resolution. We investigated the fluid velocity distribution in cylindrical and rectangular microchannels. The proposed method for measuring velocity distribution was evaluated by comparing the experiment results with a well-established theoretical solution for steady flow through the microchannels. The measurement shows that the experimental results agree well with the theoretical prediction profile. However, measurement in cylindrical channel requires special attention. For the current setup, the agreement between experimental results and theoretical prediction is much better when the detection points are scanned vertically than horizontally, mainly because of the geometrical shape and medium refractive index difference. The presented system can and will be developed for unsteady flow velocity measurement and the system parameters will be optimized in the future.

References

Aksel N, Schmidtchen M (1996) Analysis of the overall accuracy in LDV measurement of film flow in an inclined channel. Meas Sci Technol 7:1140–1147

Altria KD, Simpson CF (1987) High voltage capillary zone electrophoresis: operating parameters effects on electroendosmotic flow and eletrophoretic mobilities. Chromatographia 24:527–532

Angele KP, Suzuki Y, Miwa J, Kasagi N, Yamaguchi Y (2005) Development of a high-speed scanning micro-PIV system. In: Proceedings of 6th international symposium on particle image velocimetry, Pasadena, California, USA, September 21–23

Champion D, Hervet H, Blond G, Simotos D (1995) Comparison between two methods to measure translational diffusion of a small molecule at subzero temperature. J Agric Food Chem 43:2887–2891

Chien RL, Helmer JC (1991) Electroosmotic properties and peak broadening in field-amplified capillary electrophoresis. Anal Chem 63:1354–1361

Chiu J, Chen C, Lee P, Yang C, Chuang H, Chien S, Usami S (2003) Analysis of the effect of distributed flow on monocytic adhesion to endothelial cells. J Biomech 36:1883–1895

Dahms A, Rank R, Muller D (2007) Enhanced particle streak tracking system (PST) for two dimensional airflow patterns measurements in large planes. In: Proceedings of Roomvent 2007, Helsinki, vol 2, pp 485–492

Devasenathipathy S, Santiago J, Wereley S, Meinhart C, Takehara K (2003) Particle imaging techniques for microfabricated fluidic systems. Exp Fluids 34:504–514

Eggeling C, Widengren J, Rigler R (1998) Photobleaching of fluorescent dyes under conditions used for single-molecule detection: evidence of two-step photolysis. Anal Chem 70:2651–2659

Flamion B, Bungay PM, Gibson CC, Spring KR (1991) Flow rate measurements in isolated perfused kidney tubules by fluorescence photobleaching recovery. Biophys J C Biophys Soc 60:1229–1242

Fournier RL (2007) Basic transport phenomena in biomedical engineering. Taylor & Francis Group LLC, New York, pp 122–123

Gladden LF (2003) Magnetic resonance: ongoing and future role in chemical engineering research. AJChE J 49(1):2–9

Guenat OT, Ghiglione D, Morf WE, de Rooij NF (2001) Partial electroosmotic pumping in complex capillary systems. Part 2: Fabrication and application of a micro total analysis system (μTAS) suited for continuous volumetric nanotitrations. Sens Actuators B Chem 72:273–282

Hu H, Koochesfahani MM (2006a) Molecular tagging velocimetry and thermometry and its application to the wake of a heated circular cylinder. Meas Sci Technol 17:1269–1281

Hu H, Koochesfahani MM (2006b) A novel molecular tagging technique for simultaneous measurements of flow velocity and temperature fields. J Vis 9(4):357

Huang X, Gordon MJ, Zare RN (1988) Current-monitoring method for measuring the electroosmotic flow rate in capillary zone electrophoresis. Anal Chem 60:1837–1838

Jin S, Huang P, Park J, Yoo JY, Breuer KS (2004) Near-surface velocimetry using evanescent wave illumination. Exp Fluids 37:825–833

Kinoshita H, Oshima M, Kaneda S, Fujii T (2005) Confocal micro-PIV measurement of internal flow in a moving droplet. In: Proceedings of 9th ICMSCLS (Boston, MA), pp 629–631

Klank H, Goranovic G, Kutter J, Gjelstrup H, Michelsen J, Westergaard C (2002) PIV measurements in a microfluidic 3D-sheathing structure with three-dimensional flow behaviour. J Micromech Microeng 12:862–869

Koochesfahani MM, Nocera DG (2001) Molecular tagging velocimetry maps fluid flows. Laser Focus World 103–108

Koutsiaris A, Mathioulakis D, Tsangaris S (1999) Microscope PIV for velocity-field measurement of particle suspensions flowing inside glass capillaries. Meas Sci Technol 10:1037–1046

Kuang CF, Yang F, Zhao W, Wang GR (2008) Study on the rise time of electroosmotic flow in microcapillary tubes (submitted)

Lima R, Wada S, Tsubota K (2006) Confocal micro-PIV measurements of three-dimensional profiles of cell suspension flow in a rectangular microchannel. Meas Sci Technol 17:787–808

Liu Y, Wipf DO, Henry CS (2001) Analysis of anions in ambient aerosols by microchip capillary electrophoresis. Analyst 126:1248–1251

Manz B, Stilbs P (1995) NMR imaging of the time evolution of electroosmatic flow in a capillary. J Phys Chem 99(29):11297–11301

Meinhart C, Wereley S, Santiago J (1999) PIV measurements of a microchannel flow. Exp Fluids 27:414–419

Mosier BP, Molho JI, Santiago JG (2002) Photobleached-fluorescence imaging of microflows. Exp Fluids 33:545–554

Park JS, Choi CK, Kihm KD (2004) Optically sliced micro-PIV using confocal laser scanning microscopy (CLSM). Exp Fluid 37:105–119

Pernoder N, Tinland B (1997) Influence of λ-DNA concentration on mobilities and dispersion coefficients during agarose gel electrophoresis. Biopolymers 42:471–478

Pittman JL, Henry CS, Gilman SD (2003) Experimental studies of electroosmotic flow dynamics during sample stacking for capillary electrophoresis. Anal Chem 75:361–370

Ross D, Johnson TJ, Locascio LE (2001) Imaging of electroosmotic flow in plastic microchannels. Anal Chem 73:2509–2515

Sandoval JE, Chen SM (1996) Method for the accelerated measurement of electroosmosis in chemically modified tubes for capillary electrophoresis. Anal Chem 68:2771–2775

Sato Y, Inaba S, Hishida K, Maeda M (2003) Spatially averaged time-resolved particle-tracking velocimetry in microspace considering Brownian motion of submicron fluorescent particles. Exp Fluids 35:167–177

Schrum KF, Lancaster JM, Johnston SE, Gilman SD (2000) Monitoring electroosmotic flow by periodic photobleaching of a dilute, neutral fluorophore. Anal Chem 72:4317–4321

Shinohara K, Sugii Y, Arata A, Hibara A, Tokeshi M, Kitamori T, Okamoto K (2004) High-speed micro-PIV measurements of transient flow in microfluidic devices. Meas Sci Technol 15:1965–1970

Sinton D (2004) Microscale flow visualization. Microfluid Nanofluid 1:2–21

Sugii Y, Nishio S, Okamoto K (2002) In vivo PIV measurement of red blood cell velocity field in microvessels considering mesentery motion. Physiol Meas 23:403–416

Tallarek U, Rapp E, Scheenen T (2000) Electroosmotic and pressure-driven flow in an open packed capillaries: velocity distributions and fluid dispersion. Anal Chem 72:2292–2301

Tureci HE, Stone AD (2002) Deviation from Snell's law for beams transmitted near the critical angle: application to microcavity lasers. Opt Lett 27(1):7–9

Wanders BJ, van de Goor TAAM, Everaerts FMJ (1993) On-line measurement of electroosmosis in capillary electrophoresis using a conductivity cell. J Chromatogr A 652(1):291–294

Wang GR (2005) Laser induced fluorescence photobleaching anemometer for microfluidic devivces. Lab Chip 5:450–456

Wang GR, Sas I, Jiang H (2008) Photobleaching-based flow measurement in a commercial capillary electrophoresis chip instrument. Electrophoresis 29:1253–1263

Williams BA, Vigh G (1997) Determination of accurate electroosmotic mobility and analyte effective mobility values in the presence of charged interacting agents in capillary electrophoresis. Anal Chem 69(21):4445–4451

Wu DH, Chen AD, Johnson CS (1995) Flow imaging by means of 1D pulsed-field-gradient NMR with application to electroosmotic flow. J Magn Reson Ser A 115:123–126

Zettner CM, Yoda M (2003) Particle velocity field measurements in a near-wall flow using evanescent wave illumination. Exp Fluids 34:115–121